Estimating supermassive black hole masses in active galactic nuclei using polarization of broad Mg ii, H α, and H β lines

Đorđe Savić, L Popović, E Shablovinskaya, V Afanasiev

HAL Id: hal-03158964
https://hal.science/hal-03158964

Submitted on 4 Mar 2021

Estimating supermassive black hole masses in active galactic nuclei using polarization of broad Mg II, H α, and H β lines

Đorđe Savić [ID],[1,2]⋆ L. Č. Popović,[1,3]⋆ E. Shablovinskaya [ID][4] and V. L. Afanasiev[4]⋆

[1]*Astronomical Observatory Belgrade, Volgina 7, 11060 Belgrade, Serbia*
[2]*Observatoire Astronomique de Strasbourg, Université de Strasbourg, CNRS, UMR 7550, 11 rue de l'Université, F-67000 Strasbourg, France*
[3]*Department of Astronomy, Faculty of Mathematics, University of Belgrade, Studentski trg 16, 11000 Belgrade, Serbia*
[4]*Special Astrophysical Observatory of the Russian Academy of Sciences, Nizhnij Arkhyz, Karachaevo-Cherkesia 369167, Russia*

ABSTRACT

For type-1 active galactic nuclei (AGNs) for which the equatorial scattering is the dominant broad-line polarization mechanism, it is possible to measure the supermassive black hole (SMBH) mass by tracing the Keplerian motion across the polarization plane position angle φ. So far, this method has been used for 30 objects but only for H α emission line. We explore the possibilities of this method for determining SMBH masses using polarization in broad emission lines by applying it for the first time to Mg II $\lambda 2798$ Å spectral line. We use three-dimensional (3-D) Monte Carlo radiative transfer code STOKES for simultaneous modelling of equatorial scattering of H α, H β, and Mg II lines. We included vertical inflows and outflows in the Mg II broad-line region (BLR). We find that polarization states of H α and H β lines are almost identical and SMBH-mass estimates differ by 7 per cent. For Mg II line, we find that φ exhibits an additional 'plateau' with a constant φ, which deviates than the profiles expected for pure Keplerian motion. SMBH-mass estimates using Mg II line are higher by up to 35 per cent than those obtained from H α and H β lines. Our model shows that for vertical inflows and outflows in the BLR that are higher or comparable to the Keplerian velocity, this method can be applied as a first approximation for obtaining SMBH mass.

Key words: polarization – scattering – galaxies active – supermassive black holes.

1 INTRODUCTION

Supermassive black holes (SMBHs) reside in the heart of nearly every massive galaxy in the Universe. Their mass typically ranges between 10^6 and $10^{9.5}$ M$_\odot$ (Kormendy & Richstone 1995). Most of them lie dormant, but when the nearby gas is abundant, it will start the accretion process where the disc is formed. As the temperatures of the accreting matter increase, an immense amount of energy is radiated, triggering an active phase now known as an active galactic nucleus (AGN) (Salpeter 1964; Zel'dovich & Novikov 1964; Lynden-Bell 1969). Whether they are dormant or active, the gas and stars surrounding SMBHs are sensitive to their presence, allowing us to measure their mass. When in their active phase, SMBHs play an important role in shaping its environment in a process called AGN feedback (Fabian 2012 and references therein). As a consequence of AGN feedback, numerous correlations of SMBH mass with the properties of the host galaxy have been found, of which the most notable is $\mathcal{M}_{bh}$–σ_* relation (Kormendy & Ho 2013), implying that SMBH and the host galaxy co-evolve together (Heckman & Kauffmann 2011). Therefore, reliable SMBH-mass measuring is an important task in astronomy. For that purpose, different techniques have been developed, both direct and indirect (Peterson 2014, for more details), with most of the methods targeting AGNs due to their high luminosity, which can be readily observed at different

cosmological scales. The standard paradigm, or the so called unified model of AGNs (Antonucci 1993) assumes that the SMBH is surrounded by an accretion disc which is further away from the centre fragmented into an optically thick dusty torus. Dusty torus collimates the radiation in the polar direction and obscures the central region along the equatorial viewing direction. The broad-line region (BLR) resides in the vicinity of the SMBH, at distances of a few to a few hundred light days, in which the gas is being photoionized by the radiation from the accretion disc. Lines are emitted due to radiative recombination and collisional excitations (Netzer 2013) and their width of a few thousand km s^{-1} is due to the Keplerian motion around the SMBH (Clavel et al. 1991). The observed dichotomy between type-1 AGNs where the broad emission lines are visible and the type-2 AGNs with only narrow emission lines in their optical spectra is largely due to orientation effects where type-1 AGNs are observed from close to pole-on view while type-2 AGNs are viewed at much higher inclinations, closer towards edge-on view. For other AGN components and the unified model review, we refer to Netzer (2015).

Over the past years, the most reliable SMBH-mass measurements has come from the reverberation mapping (RM) of AGNs (Bentz & Katz 2015). By measuring the time delay between the variability of the ionizing continuum and the broad emission lines variability, we can obtain a photometric BLR radius. With known photometric radius, and the velocity measured directly from the broad emission line, we can obtain the SMBH mass (Bahcall, Kozlovsky & Salpeter 1972; Blandford & McKee 1982; Peterson 1993).The duration of an RM experiment can be rather long. An individual galaxy needs to

⋆ E-mail: djsavic@aob.rs (DS); lpopovic@aob.rs (LCP); vafan@sao.ru (VLA)

be observed over and over again for several months, while distant AGNs require several years of successful monitoring (Kaspi et al. 2000, 2007; Peterson et al. 2004; Shapovalova et al. 2009; Barth et al. 2013, 2015; Du et al. 2014, 2015, 2018; Shen et al. 2016; Grier et al. 2017, 2019; Ilić et al. 2017; Du & Wang 2019). Hydrogen Balmer lines are the most commonly used, however, lines with a range of ionization levels, like Mg II and C III], and C IV can also be used for AGNs at higher redshifts (Mejía-Restrepo et al. 2016). A few decades of intense RM campaigns have shown that photometric radius scales well with continuum luminosity, which allows us to measure the SMBH from a single-epoch optical spectrum (Peterson 2014, for a review).

Another single-epoch method that is recently proposed uses the rotation of the polarization plane position angle across the broad emission line profile in order to trace the Keplerian motion and determine the SMBH mass (Afanasiev & Popović 2015, hereafter AP15). It assumes that the BLR is flattened and the light is dominantly being scattered from the inner side of the dusty torus (equatorial scattering, Smith et al. 2005), resulting in the broad-line polarization.

The advantages and disadvantages of the AP15 method as well as comparison with the RM method were given in AP15 paper and here we will not repeat those, let us just recall several important points. This method does not a priori assume the Keplerian motion, this can be detected in the polarization angle shape. However, the method additionally requires that the distance to the scattering region (SR) is known, whether using dust RM in the infrared (Hönig 2014; Koshida et al. 2014) or measured directly using the infrared interferometry (Kishimoto et al. 2011). In the latter case, AP15 and the RM single-epoch method use different input observables, which makes it plausible to assume that these two methods are independent. Additionally, using AP15 method in combination with RM, some BLR characteristics can be determined (see for more details, Afanasiev, Popović & Shapovalova 2019).

Detailed investigation of the AP15 method by Savić et al. (2018) and Savić (2019) has shown that it can be used when outflow/inflow velocity components are present, but low. Subsequently, Afanasiev et al. (2019) have used the AP15 for a sample of 30 type-1 AGNs. The same authors have also found viewing inclinations, maximal extents of the BLR, and the index of the power-law emissivity, demonstrating that the AP15 method can be used for calibration purpose since it is in good agreement with the $\mathcal{M}_{bh}$–σ_* relation and the RM. However, the AP15 method has been applied so far only for nearby type-1 AGNs exploiting the polarization of Hα spectral line, although it could also be applied to broad emission lines like Mg II and C III], and C IV. These lines are known for their slightly blueshifted peaks and very often asymmetric profiles with a larger excess in the blue part of line. Such line profiles are very often associated with the additional BLR complex motion as radial inflows and vertical outflows (Gaskell 1982; Baskin & Laor 2005). The Mg II line is no exemption, and recently, Popović, Kovačević-Dojčinović & Marčeta-Mandić (2019) have shown that a significant inflow/outflow velocity component of a few thousand of km s^{-1} is present. Knowing that the polarization state is highly sensitive to geometry and kinematics (Goosmann & Gaskell 2007), the presence of high inflowing/outflowing components in the BLR should have a strong influence on the polarization of the Mg II line.

In order to probe the AP15 for an Mg II line, we model the equatorial scattering for Hα, Hβ, and Mg II lines, and discuss the general polarization signature. The paper is organized as follows: In Section 2, we describe the model and we list all the parameters used. Our results are given in Section 3, together with the description of

the observation procedure. Finally, we discuss the implications of our results and outline main conclusions.

2 MODEL SETUP

We apply full 3D radiative transfer with polarization using a publicly available code STOKES (Goosmann & Gaskell 2007; Marin et al. 2012; Marin, Goosmann & Gaskell 2015; Marin 2018; Rojas Lobos et al. 2018). The programme is suitable for dealing with complex geometry and kinematics of the model and treats multiple reprocessing events such as electron and dust scattering as well as dust absorption. The luminosity of the source is divided into a large number of photon packages (typically more than 10^7 per wavelength bin) and follows the input SED (power law for the continuum or Lorentz profile for the emitted broad line). For each emitted photon, the code follows its path and computes STOKES parameters I, Q, U, and V after each scattering. If there is no SR along the photon's path, the photon with its polarization state is finally registered by one of the virtual detectors in the sky. The total (unpolarized) flux (TF), polarization degree (p), and the polarization position angle φ are computed by summing STOKES parameters of all detected photons for each spectral bin. The code was originally developed for modelling optical and ultraviolet (UV) scattering induced continuum polarization in the radio-quiet AGNs, but it can be applied for studying polarization of many astrophysical phenomena (Marin & Goosmann 2014). The default output of the code $\varphi = 90°$ corresponds to a polarization state, where electrical field vector $\boldsymbol{E}$ is oscillating in the direction parallel to the axis of the symmetry of the system (z-axis). This is the opposite to the convention used by Smith et al. (2005).

2.1 Model parameters

We approximate the accretion disc emission with a point-like continuum source emitting isotropic[1] unpolarized radiation for which spectral energy distribution (SED) is given by a power law $F_C \propto \nu^{-\alpha}$. We set $\alpha = 2$, which corresponds to a flat spectrum when frequency is substituted with wavelength.

The most convenient method for finding the size of the BLR is the RM technique (Kaspi et al. 2005; Bentz et al. 2006, 2013). Savić et al. (2018) have compiled the RM measurement values found in literature for well known type-1 AGNs and their luminosities at 5100 Å (L_{5100}), and roughly estimated the BLR size (inner and outer radius) depending only on the mass of the SMBH. In this work, we set the SMBH mass to be $M_{bh} = 10^8$ M$_\odot$ and adopt the same values for the corresponding Hα BLR inner and outer radius (see Table 1). The corresponding BLR velocity is of the order of few thousands of km s^{-1}.

A systematic study by Popović et al. (2019) of 287 type-1 AGNs with broad emission lines with redshift $0.407 < z < 0.643$ (in order to include both Hβ and Mg II spectral lines), has shown that the Mg II BLR might be slightly larger than the Hβ BLR since the full width at half-maximum (FWHM) of Mg II is slightly less than the FWHM of Hβ. We set the outer size of the Mg II BLR to be 10 per cent larger than the one for Hβ. The BLR was modelled as a distribution of gas in a disc-like flattened geometry with the Keplerian motion with notable inflows and outflows present in the Mg II line. The complex structure of the BLR has been extensively

---

[1]Although the emission of a thin accretion disc is in the form cos θ, this would not affect the obtained profiles itself, however, we could expect a significant decrease in polarized flux due to seed photons having direction preference towards pole on viewing angles.

Table 1. The inner and the outer radius of the BLRs for H α, H β, and Mg II as well as for the SR. Spectral range and spectral resolution for each simulation around the central wavelengths.

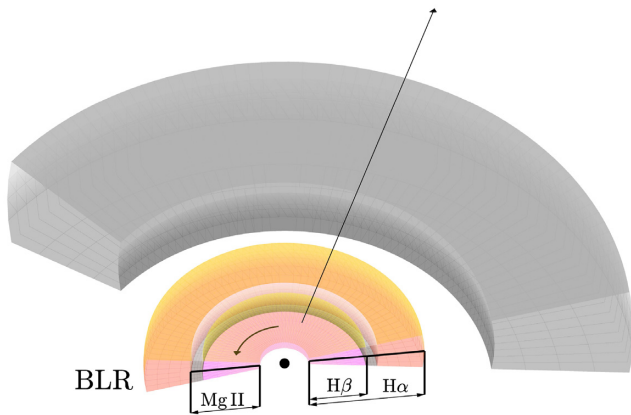|	Region	R_{in} ld	R_{out} ld	λ_{min} (Å)	λ_{max} (Å)	Spectral resolution
BLR	H α	36.94	58.93	6300	6826	300
	H β	36.94	47.91	4666	5055	300
	Mg II	36.94	50.11	2688	2912	300
SR		117.87	201.22			

Figure 1. A 3D sketch showing the model geometry and kinematics of the three (H α, H β, and Mg II) BLRs (orange) and the SR (grey). The size of each BLR is denoted with corresponding arrows and additional velocity component is accounted for the BLR of Mg II.

studied via comparison of the broad-line profiles between H β, Mg II, and other spectral lines (Kovačević-Dojčinović & Popović 2015, and references therein). The RM measurements of optical Balmer lines for nearby type-1 AGNs (Bentz et al. 2010) have shown that for most of the objects, the H α BLR is larger than the H β BLR. From a much larger RM sample of type-1 AGNs, the size of the Mg II BLR is consistently slightly larger than the size of the H β BLR (Shen et al. 2016), which is in agreement with H β being slightly more variable than Mg II line (Sun et al. 2015). For the sake of the model, in order to reduce the number of free parameters concerning the size of each BLR, we fix the size of the H β BLR to be 50 per cent the size of the H α BLR and Mg II BLR to be 60 per cent the size of H α BLR (Fig. 1). The half opening angle for the BLR is 30°, which corresponds to the covering factor $CF_{BLR} = 0.5$. We assume that the BLR is transparent i.e. we neglect the line scattering by the BLR itself since the optical depth for Thomson scattering in our case is $\tau_{BLR} = 0.04R_{0.1\,pc}$, where $R_{0.1\,pc} = R_{BLR}/0.1$ pc (Songsheng & Wang 2018). For all three regions, the Keplerian motion is included. Only for the Mg II, constant 6000 km s^{-1} inflow and outflow velocity component was added for the innermost one third of the region at an angle of 60° with respect to the equatorial plane.[2]

In the work by Savić et al. (2018), it was found that the SR requires much higher covering factor and higher radial optical depth than the one used by Smith et al. (2005) in order to produce the polarization signal typically observed in type-1 AGNs. Assuming that the equatorial scattering occurs only from the inner part of the

[2]Only the inflow/outflow velocity component was added while the same geometry of the Mg II region was kept.

torus, we adopt the same values for the SR radial thickness as given by Savić et al. (2018) with the total radial optical depth equal to 1 for Thomson scattering. The half opening angle for the SR is 35°, which corresponds to $CF_{SR} = 0.57$. The best SMBH-mass estimates using polarization of broad emission lines are when the ratio between the SR inner radius and the BLR outer radius $R_{SR}^{in}/R_{BLR}^{out}$ is between 1.5 and 2.5. A value of 1.72 ± 0.48 for this ratio has been obtained by Afanasiev et al. (2019). Therefore, we set the SR to be at twice the distance of the H α BLR when measured from the centre. List of all model parameters is given in the Table 1. An illustration of the model geometry is shown in Fig. 1. We performed three separate simulations covering each of the Mg II, H β, and H α spectral domains.

3 RESULTS

In this section, we compare polarization and line profiles for H α, H β, and Mg II lines. The equatorial scattering dominates the systems with inclination range between 20° and 70°. We restrict viewing inclinations for type-1 objects, which is in our case between 20° and 55°.

In Fig. 2 (top panels), the profiles for φ for each line and for four viewing inclinations are shown. We can see that the φ-profiles for H α and H β are nearly identical in the wings, while in the core, the position of the φ amplitude (maximal offset from the continuum level which is $\varphi_{cont} = 90°$) is for H α slightly shifted towards the core for roughly 500 km s^{-1}. This is expected since the H α BLR is larger than the H β BLR. The φ amplitude for Mg II is around 5° lower than the amplitudes for H α and H β. In the wings, the φ amplitude for Mg II is showing a 'plateau' rather than following profiles for pure Keplerian motion.

In Fig. 2 (second row from the top), the results for simulated p are shown. The double-peaked profile mentioned before is present for all three spectral lines. The p profiles for H α and H β are almost the same. The p profile for Mg II shows lower polarization in the wings and slightly higher in the core than the p for H α and H β. The p maxima for Mg II are shifted towards blue for approximately 1000 km s^{-1} with respect to the maxima for the p of H β when viewed from the lowest viewing inclination (Fig. 2, second row from the top, first column from the left). This shift of the maximum p between Mg II and H β (or H α) is decreasing when the system is viewed from intermediate inclinations since the effects of the inflows and outflows are the greatest for the pole-on view.

In Fig. 2 (third row from the top), the results for simulated polarized flux (PF) are shown for all four viewing inclinations. Polarized lines look very similar for all three lines except that the polarized Mg II line is slightly stronger in the wings. In this case, the SR can fully resolve the Keplerian motion in the BLR, while the influence of the inflows and outflows present in the Mg II region is minor since the projection of the inflow or outflow velocity component in any direction towards the SR is much smaller in comparison with the Keplerian velocity. The polarized lines get broader when viewed from pole-on view towards the more inclined viewing angles and show a clear double-peaked profiles.

The results for unpolarized lines are shown in Fig. 2 (bottom panels). All profiles are single-peaked and broader when viewed from pole-on towards higher viewing inclinations. The profiles for H α and H β lines are almost the same. The FWHM of H α line is less than the FWHM of H β by 500 km s^{-1}. This might be counter-intuitive since the H α BLR is twice the size of the H β BLR. The reason is that for our model setup, the velocity difference between the outer parts of the H β and H α BLRs is only 300 km s^{-1}, which combined with the inclination effects give slightly broader H β than H α line. The effects of inflows and outflows present in the Mg II region is
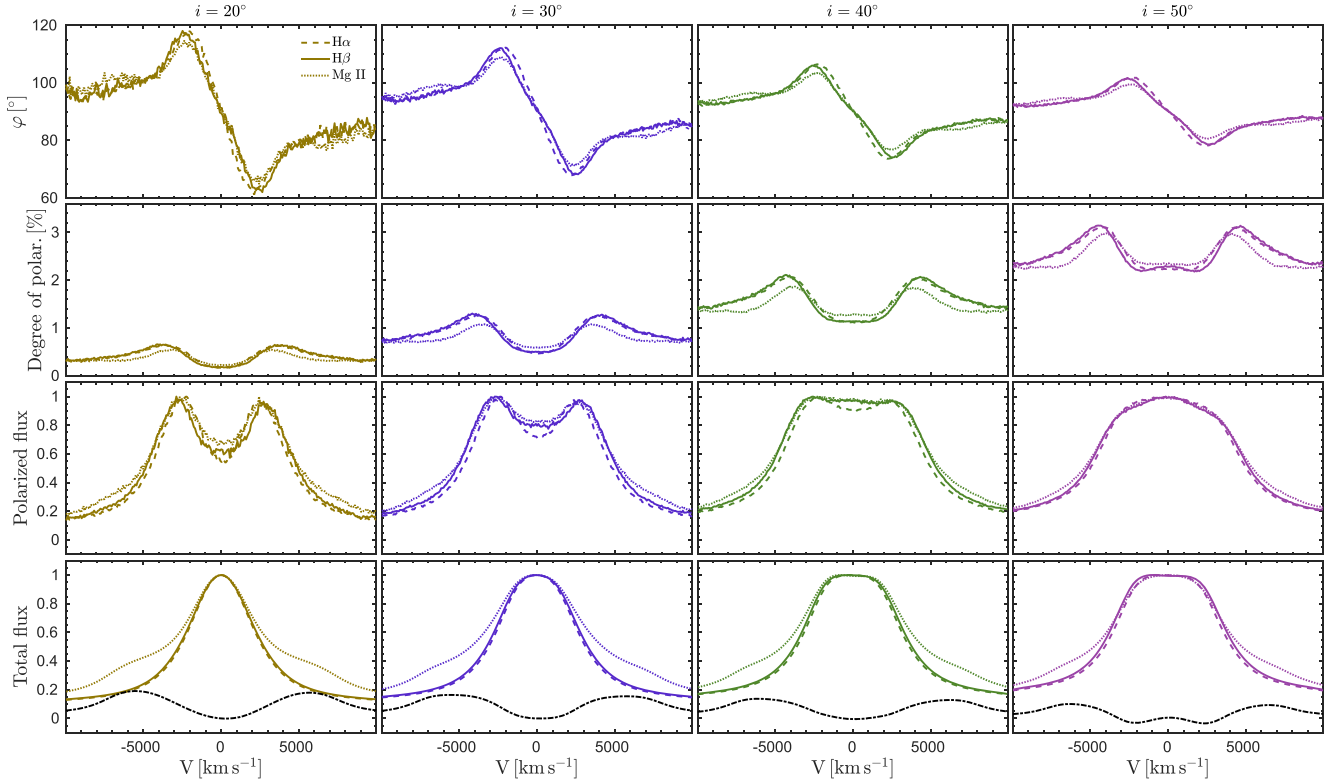
Figure 2. Polarization signature of each line for four viewing inclinations. Line styles correspond to the following order: Dash–dotted line is for H α, solid line for H β, and dotted line for Mg II. The φ-profiles (top panels), degree of polarization (second row from the top), polarized flux (third row from the top), and total flux (bottom panels) are shown with respect to velocity. Dashed black lines (bottom panels) represent the difference between the Mg II and H β unpolarized flux. Columns from the left-hand side to the right-hand side correspond to viewing inclination in ascending order, from near face-on towards intermediate inclinations.

clearly visible in the strong wings of the Mg II line profile. Strong wings directly influence the p profiles ($p = $ PF/TF) by reducing net polarization in the Mg II line. The comparison between the H β and Mg II lines is shown in Fig. 2 (bottom panels, dash–dotted line). It shows a symmetric double-peaked feature, very similar to the results by Popović et al. (2019) for the SDSS sample. We point out that the unpolarized lines are symmetric since the BLR is transparent in our model and we observe radiation from both sides of the equatorial plane instead of observing only the radiation coming from the side closer to the observer. Thus, both blue and red wings of the Mg II lines are prominent instead of having blue asymmetry that corresponds to a more realistic geometry.

The QU-plane for H β and Mg II line is shown in Fig. 3 for four viewing inclinations. In the same figure (upper rightmost panel), the evolution of the Q and U parameters along the line is indicated by blue arrows. The U parameter starts around values close to zero and then it evolves giving rise to φ. When $\varphi_{\max}$ is reached, U increases almost vertically and gets positive when line centre is crossed. The opposite pattern is then followed in the red part of the line. In line wings, we can see that there is a clear distinction between the two groups of points for H β and Mg II. The distance of each point from the centre corresponds to p. Since p in the wings is higher for H β than for Mg II (Fig. 2, second from top panels), the Q and U parameters for H β encompass the Q and U for Mg II in the QU-plane.

3.1 Mass estimates

The model predicts S-shaped profile of the polarization angle (Fig. 2, top panels), which reflects Keplerian-like motion when the equatorial

scattering is a dominant scattering mechanism. Then, as it was shown in Afanasiev et al. (2014) and Afanasiev & Popović (2015), velocity V and polarization plane position angle φ are connected by the following relation:

$$\log\left(\frac{V}{c}\right) = a - b \times \log(\tan[\Delta\varphi]), \tag{1}$$

where c is the speed of light, $\Delta\varphi = \varphi - \langle\varphi\rangle$ is the difference between the polarization angle and its mean value, and a and b are the coefficients of the linear approximation. The coefficient b is equal to 0.5 as we assume the Keplerian-like motion. It is known that a is connected with the BH mass $\mathcal{M}_{bh}$ as

$$a = 0.5 \log\left(\frac{G\mathcal{M}_{bh}\cos^2(\theta)}{c^2 R_{sc}}\right), \tag{2}$$

where G is the gravitational constant, R_{sc} is the distance from the central BH to the SR, and θ is an angle between the BLR and the SR.

In Fig. 4, we show φ-profiles and linear fits using the equation 1 for all three spectral lines [H α (top panels), H β (middle panels), and Mg II (bottom panels)] and for four viewing inclinations (from left to right). We can see that for H α and H β lines we obtain good linear fit, and mass estimates are close to an input mass of $10^8 \, \mathrm{M}_\odot$. Mass estimates from H β are systematically slightly higher than masses obtained from H α polarization angle profiles, owing to the H β emission region having velocities that are up to $500 \, \mathrm{km \, s^{-1}}$ higher than the velocities of the H α emission region. In the case for Mg II line, the $\log(V/c) - \log\tan\Delta\varphi$ dependence significantly deviates from a linear relation. We can see that a linear relation (the Keplerian motion) is valid only in the narrow velocity part between the peak and the plateau, which for our case corresponds to
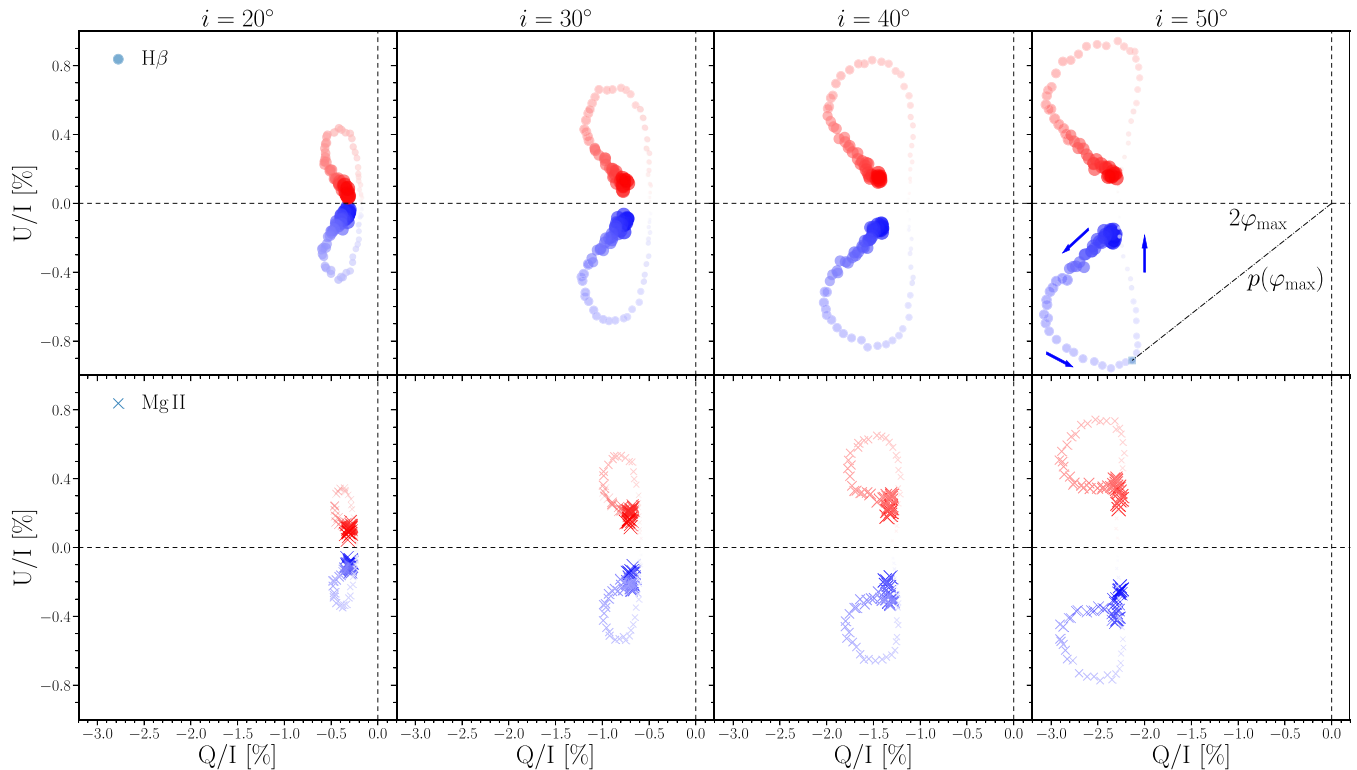
Figure 3. *QU*-plane for H β (circles, upper panels) and Mg II (crosses, lower panels) normalized with *I*. Size and shade of symbols correspond to velocity in such a way that greater size and darker shade correspond to higher velocities. Red denotes velocity greater than zero, while blue is the opposite. Dashed black lines are constant zero values of *Q* and *U*. Panels from left- to right-hand side are for four viewing inclinations. On the upper rightmost panel, blue arrows denote the direction of *Q* and *U* across the line profile. Blue square correspond to φ_{max} for H β line. The angle between the dash–dotted line and the $U = 0$ is $2\varphi_{max}$. The distance from the coordinate system origin represents *p*. Different symbols for H β (circles) and Mg II (crosses) were used for contrast highlighting.

velocities between 2500 and 4500 km s^{-1} in both red and blue part of the line. The plateau covers the velocity range 4500–6500 km s^{-1} and a constant value of $\Delta\varphi$. This gives a vertical rise in the log (*V/c*) − log tan $\Delta\varphi$, before $\Delta\varphi$ values finally drop to zero in the far wings. The Keplerian part almost matches the 1σ uncertainties when all points are used in the linear fit. If we perform linear fit only for these points, estimated SMBH masses are ∼35 per cent lower. From the observational point of view, the resolution is much worse and the data points are typically much more scattered around the straight line (Afanasiev et al. 2019) and observing φ-profiles similar to the modelled Mg II φ-profile would be difficult. Therefore, in a first approximation, we can perform a linear fit of the whole data set obtained from the observations of the polarized Mg II line, and assign additional 35 per cent uncertainty to the estimated mass. That way the obtained SMBH masses would still be of the same order with the masses estimated from the φ- profiles of H α or H β lines where no or low velocity outflows are present. The exact values of parameter *a* and SMBH masses obtained for linear fits using all points and for each viewing inclination are given in Table 2.

4 DISCUSSION

We investigated polarization effects in all three broad lines, focusing on the Mg II line and the application of the AP15 method. The polarized lines have almost the same profiles and widths, for all three emission lines, even for such high inflows and outflows present in the Mg II BLR. The reason is that the emitted BLR radiation is seen by scatterers at close to edge-on viewing angles, and the projected

vertical velocity component becomes low. The H β and H α lines show almost identical φ, *p*, PF, and TF profiles with differences in broadening effects of the order of 500 km s^{-1}. SMBH-mass estimates using H β are ∼7 per cent higher than the one obtained using H α due to the smaller size of the H β region. The Mg II emission line shows a plateau of constant φ before dropping to the continuum value φ_c in the extreme line wings. In a first attempt, SMBH-mass estimates from the Mg II emission line with extreme outflows would have additional ∼35 per cent error when compared with results obtained by using AP15 method for H α and H β, which are still in agreement with previous results.

Single-epoch SMBH-mass estimates using Mg II and C IV are of great importance for highly redshifted AGNs (see review, Popović 2020 and references therein). Typically, SMBH mass using these lines is derived from the $L_{5100} - R_{BLR}$ relation for H β line (Vestergaard & Peterson 2006; Wang et al. 2009; Trakhtenbrot & Netzer 2012; Marziani et al. 2013a,b; Mejía-Restrepo et al. 2016; Popović et al. 2019). If the emission of the Mg II line is dominated by the virialized component, we could expect a good agreement between the SMBHs obtained using the AP15 and the single-epoch SMBH-mass estimates using Mg II line. However, a considerable amount of objects show systematically blueshifted and asymmetric Mg II line profiles which are dominated by a non-virial kinematics (Mejía-Restrepo et al. 2016) and for which the FWHM > 6000 km s^{-1} (Popović et al. 2019). For these objects, we could expect much different geometry than the simple one we used.

When comparing the AP15 method with the single-epoch SMBH-mass estimates using FWHM, it is commonly assumed that the BLR gas is virialized in the vicinity of the BH. This may not always
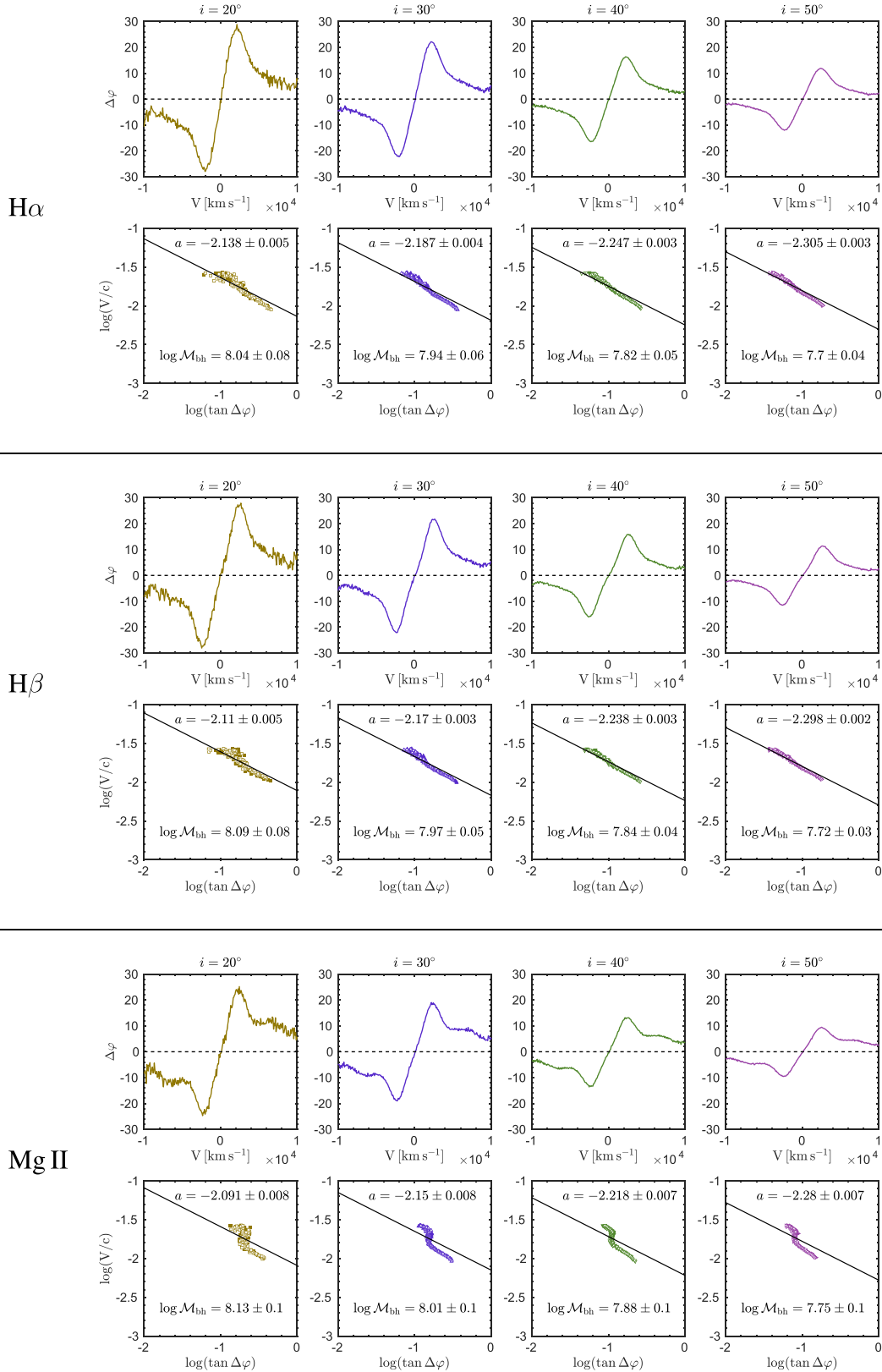
Figure 4. SMBH-mass estimates from the φ of Hα (top panels), Hβ (middle panels), and Mg II (bottom panels). From left- to right-hand side are viewing inclinations starting from $20°$, $30°$, $40°$, and $50°$. For each line, panels are divided into two parts: Upper part is φ-profiles; lower part: $\log(V/c) - \log\tan\Delta\varphi$ linear fit. Empty and filled symbols in the lower part are for blue and red part of the line, respectively.

Table 2. SMBH-masses estimated from Hα, Hβ, and Mg II lines for four viewing inclinations. Spectral line (column 1), viewing inclinations (column 2), parameter a (column 3), obtained masses given in $M_\odot$ (column 4), and estimated mass divided by input mass $\mathcal{M}_{\text{input}} = 10^8\,M_\odot$ (column 5).

Line	$i(°)$	a	$\log(\mathcal{M}_{\text{bh}}/M_\odot)$	$\mathcal{M}_{\text{bh}}/\mathcal{M}_{\text{input}}$
Hα	20	-2.138 ± 0.005	8.04 ± 0.08	1.09
	30	-2.187 ± 0.004	7.94 ± 0.06	0.87
	40	-2.247 ± 0.003	7.82 ± 0.05	0.66
	50	-2.305 ± 0.003	7.70 ± 0.04	0.50
Hβ	20	-2.110 ± 0.005	8.09 ± 0.08	1.23
	30	-2.170 ± 0.003	7.97 ± 0.05	0.93
	40	-2.238 ± 0.003	7.84 ± 0.04	0.69
	50	-2.298 ± 0.002	7.72 ± 0.03	0.52
Mg II	20	-2.091 ± 0.008	8.13 ± 0.10	1.35
	30	-2.150 ± 0.008	8.01 ± 0.10	1.02
	40	-2.218 ± 0.007	7.88 ± 0.10	0.76
	50	-2.280 ± 0.007	7.75 ± 0.10	0.56

be the case due to the uncertain gas distribution or the presence of the outflowing winds of various origin (León-Tavares et al. 2013; Mejía-Restrepo et al. 2018). These effects can be observed in the polarized spectra, which is the advantage of the AP15 method, however, observational evidence still needs to be confirmed.

Lira et al. (2020) have included large $3000\,\text{km}\,\text{s}^{-1}$ bulk outflows in the SR. They showed that such configuration greatly affects the observed φ-profiles which deviate from the one obtained for pure Keplerian motion. In our model, we did not include complex motions of the SR since it is sufficiently far enough for outflowing velocities to be comparable with the Keplerian velocity that is around $2000\,\text{km}\,\text{s}^{-1}$. Low-magnitude inflows/outflows can be neglected (Savić et al. 2018).

5 CONCLUSION

We assumed the equatorial scattering of the inner side of the dusty torus to be the main UV/optical broad-line polarization mechanism. We used the 3D Monte Carlo radiative transfer code STOKES for accurate polarization treatment. We modelled equatorial scattering simultaneously for Hα, Hβ, and Mg II emission lines.

From the results obtained in this work, we may conclude the following:

(i) The presence of vertical inflows and outflows in the BLR that is much higher than the Keplerian velocity produces a plateau in the polarization plane position angle profiles.

(ii) The application of the AP15 method is valid as a rough first approximation even for the extreme outflows of the BLR.

(iii) Error obtained this way is around $\sim$35 per cent.

We have paved the way for the use of the AP15 method for highly ionized lines. For the future work, we plan to observe a few objects covering Mg II and C III], C IV, and Lα spectral range, and compare the SMBH-mass estimates with other single-epoch methods in order to obtain more general results.

DATA AVAILABILITY STATEMENT

Data in this paper are available on request. The data underlying this article will be shared on reasonable request to the corresponding author.

REFERENCES

Afanasiev V. L., Popović L. Č., 2015, ApJ, 800, L35 (AP15)
Afanasiev V. L., Popović L. Č., Shapovalova A. I., Borisov N. V., Ilić D., 2014, MNRAS, 440, 519
Afanasiev V. L., Popović L. Č., Shapovalova A. I., 2019, MNRAS, 482, 4985
Antonucci R., 1993, ARA&A, 31, 473
Bahcall J. N., Kozlovsky B.-Z., Salpeter E. E., 1972, ApJ, 171, 467
Barth A. J. et al., 2013, ApJ, 769, 128
Barth A. J. et al., 2015, ApJS, 217, 26
Baskin A., Laor A., 2005, MNRAS, 356, 1029
Bentz M. C., Katz S., 2015, PASP, 127, 67
Bentz M. C. et al., 2006, ApJ, 651, 775
Bentz M. C. et al., 2010, ApJ, 716, 993
Bentz M. C. et al., 2013, ApJ, 767, 149
Blandford R. D., McKee C. F., 1982, ApJ, 255, 419
Clavel J. et al., 1991, ApJ, 366, 64
Du P., Wang J.-M., 2019, ApJ, 886, 42
Du P. et al., 2014, ApJ, 782, 45
Du P. et al., 2015, ApJ, 806, 22
Du P. et al., 2018, ApJ, 856, 6
Fabian A. C., 2012, ARA&A, 50, 455
Gaskell C. M., 1982, ApJ, 263, 79
Goosmann R. W., Gaskell C. M., 2007, A&A, 465, 129
Grier C. J. et al., 2017, ApJ, 851, 21
Grier C. J. et al., 2019, ApJ, 887, 38
Heckman T. M., Kauffmann G., 2011, Science, 333, 182
Hönig S. F., 2014, ApJ, 784, L4
Ilić D. et al., 2017, Frontiers Astron. Space Sci., 4, 12
Kaspi S., Smith P. S., Netzer H., Maoz D., Jannuzi B. T., Giveon U., 2000, ApJ, 533, 631
Kaspi S., Maoz D., Netzer H., Peterson B. M., Vestergaard M., Jannuzi B. T., 2005, ApJ, 629, 61
Kaspi S., Brandt W. N., Maoz D., Netzer H., Schneider D. P., Shemmer O., 2007, ApJ, 659, 997
Kishimoto M., Hönig S. F., Antonucci R., Millour F., Tristram K. R. W., Weigelt G., 2011, A&A, 536, A78
Kormendy J., Ho L. C., 2013, ARA&A, 51, 511
Kormendy J., Richstone D., 1995, ARA&A, 33, 581
Koshida S. et al., 2014, ApJ, 788, 159
Kovačević-Dojčinović J., Popović L. Č., 2015, ApJS, 221, 35
León-Tavares J. et al., 2013, ApJ, 763, L36
Lira P., Goosmann R. W., Kishimoto M., Cartier R., 2020, MNRAS, 491, 1
Lynden-Bell D., 1969, Nature, 223, 690
Marin F., 2018, A&A, 615, A171
Marin F., Goosmann R. W., 2014, in Ballet J., Martins F., Bournaud F., Monier R., Reylé C., eds, Proc. SF2A-2014, Ten Years of Radiative Transfer with STOKES. SAF, Paris, p. 103

Marin F., Goosmann R. W., Gaskell C. M., Porquet D., Dovčiak M., 2012, A&A, 548, A121

Marin F., Goosmann R. W., Gaskell C. M., 2015, A&A, 577, A66

Marziani P., Sulentic J. W., Plauchu-Frayn I., del Olmo A., 2013a, A&A, 555, A89

Marziani P., Sulentic J. W., Plauchu-Frayn I., del Olmo A., 2013b, ApJ, 764, 150

Mejía-Restrepo J. E., Trakhtenbrot B., Lira P., Netzer H., Capellupo D. M., 2016, MNRAS, 460, 187

Mejía-Restrepo J. E., Lira P., Netzer H., Trakhtenbrot B., Capellupo D. M., 2018, Nature Astron., 2, 63

Netzer H., 2013, The Physics and Evolution of Active Galactic Nuclei, Cambridge Univ. Press, Cambridge

Netzer H., 2015, ARA&A, 53, 365

Peterson B. M., 1993, PASP, 105, 247

Peterson B. M., 2014, Space Sci. Rev., 183, 253

Peterson B. M. et al., 2004, ApJ, 613, 682

Popović L. Č., Kovačević-Dojčinović J., Marčeta-Mandić S., 2019, MNRAS, 484, 3180

Popović L. Č., 2020, Open Astron., 29, 1

Rojas Lobos P. A., Goosmann R. W., Marin F., Savić D., 2018, A&A, 611, A39

Salpeter E. E., 1964, ApJ, 140, 796

Savić D., 2019, Int. J. Cosmol., 1, 50

Savić D., Goosmann R., Popović L. Č., Marin F., Afanasiev V. L., 2018, A&A, 614, A120

Shapovalova A. I. et al., 2009, New Astron. Rev., 53, 191

Shen Y. et al., 2016, ApJ, 818, 30

Smith J. E., Robinson A., Young S., Axon D. J., Corbett E. A., 2005, MNRAS, 359, 846

Songsheng Y.-Y., Wang J.-M., 2018, MNRAS, 473, L1

Sun M. et al., 2015, ApJ, 811, 42

Trakhtenbrot B., Netzer H., 2012, MNRAS, 427, 3081

Vestergaard M., Peterson B. M., 2006, ApJ, 641, 689

Wang J.-G. et al., 2009, ApJ, 707, 1334

Zel'dovich Y. B., Novikov I. D., 1964, Sov. Phys. Dokl., 9, 246

This paper has been typeset from a TEX/LATEX file prepared by the author.